Nesting mechanism for *d*-symmetry superconductors

J. Ruvalds, C. T. Rieck,* S. Tewari, and J. Thoma
Physics Department, University of Virginia, Charlottesville, Virginia 22901

A. Virosztek
Research Institute for Solid State Physics, 1525 Budapest 114, POB 49, Hungary
(Received 29 August 1994; revised manuscript received 16 December 1994)

A nested Fermi surface with nearly parallel orbit segments is found to yield a singlet *d*-wave superconducitng state at high temperatures for a restricted range of the on-site Coulomb repulsion that avoids the competing spin-density-wave instability. The computed superconducting transition temperature drops dramatically as the nesting vector is decreased, in accord with recent photoemission data on the Bi2212 and Bi2201 cuprates. Superconducting transition temperatures in the 100 K range are produced by the nesting mechanism in the *leading order* pairing interaction caused by exchange of spin fluctuations.

I. INTRODUCTION

Even though the BCS theory[1] provides a successful description of conventional superconductors, the concept of alternate electron pairing states of finite angular momentum has evolved from the original proposal by Anderson and Morel[2] to encompass various physical systems. Spin fluctuations suppress[3,4] the BCS isotropic pair binding induced by phonon exchange, and hence materials with strong repulsive interactions are prospects for alternate pairing mechanisms. Superfluid He^3 exhibits *p*-wave pairing,[5] and heavy Fermion superconductors offer another unconventional case at very low temperatures. Berk and Schrieffer[4] found that the exchange of spin fluctuations in a Fermi liquid provides a destructive influence for *d*-wave pairing as well as for conventional *s*-wave states. The random-phase approximation (RPA) series[4] in the spin susceptibility further diminishes the possibility of generating *d*-wave pairing in a Fermi liquid characterized by a free-electron energy dispersion.

Copper oxides with high superconducting transition temperatures T_c exhibit abnormal electrical transport and optical properties. Figure 1 shows a plot of the transition temperature of various superconductors versus the power-law exponent n of the normal-state resistivity as a function of temperature, $\rho \sim T^n$. The conventional T^5 behavior arising from electron-phonon interactions in metals such as Pb and Nb is well known. The T^2 variation in the Ce-doped cuprates and various organic metals is reminiscent of electron-electron scattering in a Fermi liquid. It is remarkable that the widely observed anomalous linear temperature variation (i.e., $n=1$) of the resistivity occurs in all of the highest-T_c copper oxides. This latter correlation provides the primary theoretical challenge in the present analysis.

A linear temperature dependence of the damping was attributed by Lee and Read[6] to electron-electron collisions on a perfectly nested square Fermi surface that has a logarithmic Van Hove singularity in the density of states. A microscopic theory based on a nested Fermi liquid (NFL) produces the anomalous linear temperature variation of the resistivity[7] and also explains the surprising linear frequency variation of the quasiparticle damping[8] that is compatible with the ubiquitous infrared spectra on cuprates. The cuprate reflectance data differs substantially from standard Drude behavior.

The correlation of high-T_c values in cuprates with

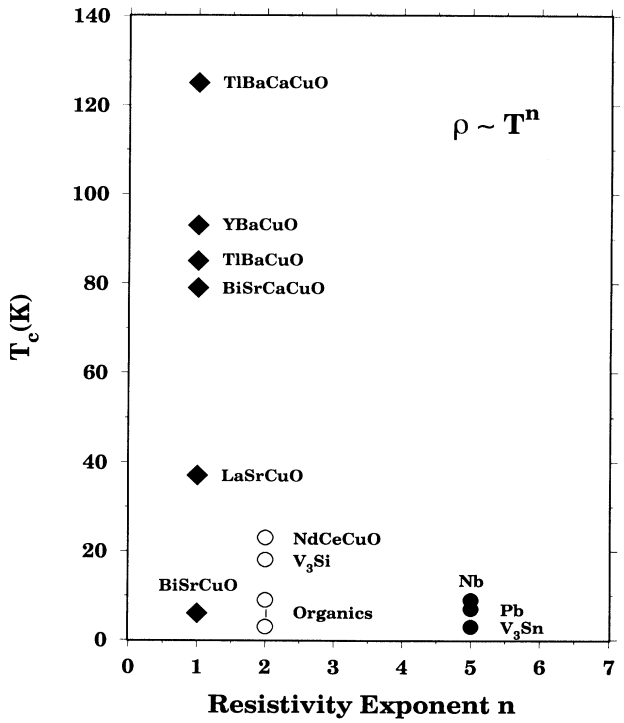

FIG. 1. The transition temperature of various superconductors is plotted vs the power-law exponent n of the normal-state resistivity $\rho = T^n$, where T is the temperature. Conventional metals such as Pb and Nb which are BCS superconductors display a T^5 dependence, while the Ce-doped (electron-doped) superconductors show a T^2 behavior. The cuprate superconductors with the highest-T_c values have a normal-state resistivity that is linear in temperature. Note in particular the difference in transition temperatures between the Bi2212 ($T_c = 80$ K) and Bi2201 ($T_c = 6$ K) cuprates.

0163-1829/95/51(6)/3797(9)/$06.00

departures from the standard Fermi-liquid behavior suggests that the physical origin of the anomalous damping may be a key source of the superconductivity. The purpose of the present study is to show that Fermi surface nesting in the form of parallel orbit segments can generate a strong attractive pairing in the d-wave channel through the exchange of spin fluctuations in leading order. The Coulomb repulsion U provides the primary interaction, while the nested orbit topology is the key determinant of the attraction strength. The spin susceptibility χ plays an important role in the pairing and nesting produces peaks in the susceptibility at the nesting vector $\mathbf{Q}^*$ that connects parallel segments of the Fermi surface. While this peak structure enhances the pairing interaction, it also drives the system closer to a spin-density-wave (SDW) instability. We thus restrict the values of the Coulomb interaction strength U to avoid the SDW instability condition $U\chi=1$.

We find that the superconducting state of d angular-momentum symmetry is favored in the $Bi_2Sr_2CaCu_2O_8$ (Bi2212) cuprate on the basis of a model energy band that yields the nested Fermi surface shown in Fig. 2. Photoemission evidence for nesting has been discovered by Dessau *et al.*[9] and Shen *et al.*,[10] and their high-resolution spectra also indicate an anisotropic gap that appears to be compatible with a d-wave state. Our computations of the superconducting transition temperature reveal a sensitivity to the extent of nesting of the Fermi surface as well as the magnitude of the nesting vector. This can account for the difference in transition temperatures observed in the Bi2212 and $Bi_2Sr_2CuO_6$ (Bi2201) cuprates, as we show below.

Scalapino *et al.*[11] found that a two-dimensional tight-binding energy band in a Hubbard model may give rise to an attractive d-wave pairing interaction, whose magnitude could be elevated by RPA corrections to the spin-fluctuation graphs. Similar pairing correlations were found in Monte Carlo simulations[12] on a small lattice. However, for the band fillings and Fermi-surface topologies treated by Scalapino[11] and others,[13–15] the lowest-order estimates give very small T_c values; and the self-energy and vertex corrections need to be considered on the same footing as the RPA series. Other anisotropic pairing proposals have been applied to organic compounds[16] and heavy Fermion superconductors.[17]

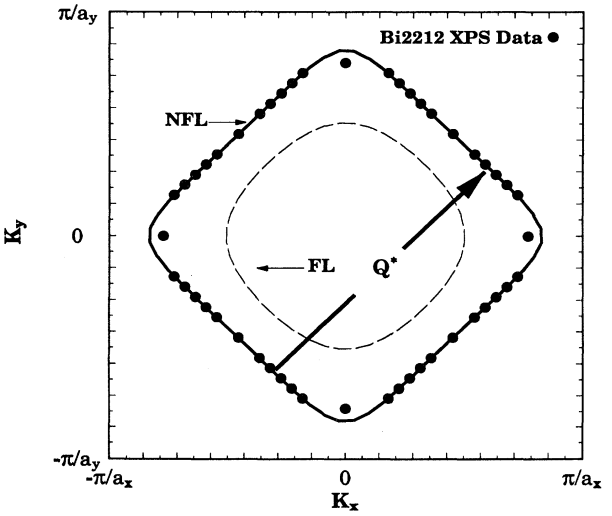

FIG. 2. A nested Fermi surface (NFL) shown by the solid curve was calculated to fit the photoemission data points of Dessau *et al.* (Ref. 10) using the tight-binding model of Eq. (2) with $B=0.165$ and $\mu=-0.56$. The nesting vector is $\mathbf{Q}^*\simeq 0.91(\pi,\pi)$ in this case. By contrast, the dashed curve for the same value of B but a chemical potential $\mu=-1.6$ shows a rounded orbit reminiscent of a standard Fermi liquid (FL).

In the next section, we present our energy band model formulated on the basis of photoemission experiments on the Bi2212 cuprate. Using this model, we present our calculated results for the spin susceptibility. In Sec. III, we discuss the conditions for superconductivity in the cuprates. We also compare our model predictions of the transition temperature for the Bi2212 and Bi2201 compounds.

II. SUSCEPTIBILITY

We consider the Hubbard Hamiltonian

$$H=\sum_{\mathbf{k},\sigma} E(\mathbf{k})c^{\dagger}_{\mathbf{k},\sigma}c_{\mathbf{k},\sigma}+U\sum_{\mathbf{p},\mathbf{q},\mathbf{k}} c^{\dagger}_{\mathbf{p}+\mathbf{q},\uparrow}c_{\mathbf{p},\uparrow}c^{\dagger}_{\mathbf{k}-\mathbf{q},\downarrow}c_{\mathbf{k},\downarrow}\ , \quad (1)$$

where the electron (or hole) energy band $E(k)$ is represented by the tight-binding expression

$$E(\mathbf{k})=-2t\left[\cos k_x+\cos k_y-B\cos k_x\cos k_y+\frac{\mu}{2}\right]. \quad (2)$$

Here U is the Coulomb repulsion between electrons at a given site, and $c^{\dagger}_{\mathbf{k},\sigma}$ ($c_{\mathbf{k},\sigma}$) represent creation (destruction) operators of momentum k and spin σ. The Fermi surfaces for this model are shown in Figure 2. A rounded orbit such as the dashed curve would produce Fermi-liquid (FL) phenomena including an electron damping that is proportional to T^2 and ω^2, where ω is the frequency. The nested surface shown by the solid curve resembles the experimental photoemission data points obtained by Dessau *et al.*[9] and Shen *et al.*[10] on $Bi_2Sr_2CaCu_2O_8$. The bandwidth $W=8t$ is estimated to be 1.5 eV from the photoemission data.

In order to investigate electron pairing mediated by the exchange of spin fluctuations, we compute the susceptibility for the energy band model of Eq. (2). Neglecting self-energy corrections, the lowest-order real part of the susceptibility, $\chi'(\mathbf{q},\omega)$, has the standard definition

$$\chi'(\mathbf{q},\omega)=\int\frac{d^2k}{(2\pi)^2}\frac{f(\mathbf{k})-f(\mathbf{k}+\mathbf{q})}{\omega-E(\mathbf{k}+\mathbf{q})+E(\mathbf{k})}\ , \quad (3)$$

where $f(\mathbf{k})=f[E(\mathbf{k})]$ is the Fermi function. The calculated susceptibility is plotted in Fig. 3 for model parameters corresponding to the two Fermi surfaces shown in Fig. 2. The dashed curve in Fig. 3 represents the Bi2212 case and the solid curve the Fermi-liquid case. Also shown is the susceptibility for the Bi2201 cuprate (dot-dashed curve). For the latter case, the model parameters

are determined from a fit to the Bi2201 Fermi surface seen in photoemission experiments by King *et al.*[18] This surface is also nested, but with a smaller nesting vector. The susceptibility peaks are significantly enhanced in magnitude and narrowed as a result of nesting, as seen in Fig. 3 which shows the static susceptibility as a function of momentum $|\mathbf{q}|$ along the $q_x=q_y$ direction. The peaks in the susceptibility are located at the nesting vector $\mathbf{Q}^*$ that spans the parallel segments of the Fermi surface. When plotted in q_x, q_y space, the three-dimensional structure of $\chi'(\mathbf{q},\omega)$ consists of four peaks, located at the following points: $\mathbf{Q}_1=(\xi\pi,\pi)$, $\mathbf{Q}_2=(\pi,\xi\pi)$, $\mathbf{Q}_3=(2\pi-\xi\pi,\pi)$, and $\mathbf{Q}_4=(\pi,2\pi-\xi\pi)$, with $\xi=0.91$ for the Bi2212 model parameters. As the orbit becomes smaller and more rounded, the peaks in the susceptibility spread apart and are greatly reduced in magnitude. Extensive calculations[19] of the spin dynamics for tight-binding models have provided quantitative insight into understanding of the NMR spectra as well as the neutron-scattering data in cuprates. In the limiting case of a free-electron energy dispersion in two dimensions, the static susceptibility is constant up to $2k_F$, where k_F is the Fermi momentum. The latter (FL) example is a case in which spin fluctuations suppress superconductivity in the d-wave as well as in the s-wave state.[4]

Virosztek and Ruvalds[7] showed that a self-consistent calculation of the susceptibility for a nested Fermi liquid gave rise to an anomalous quasiparticle damping, of the form $\Gamma\propto T$ for $|\omega|<T$ and $\Gamma\propto|\omega|$ for $|\omega|>T$, where T is the temperature and ω the frequency. Taking these NFL self-energy corrections into account, we compute the real part of the susceptibility as defined in Ref. 20,

$$\chi'(\mathbf{q},\omega)=\frac{1}{(2\pi)^3}\int d\omega'\int d\mathbf{k}[\mathrm{Im}G(\mathbf{k},\omega')\mathrm{Re}G(\mathbf{k}-\mathbf{q},\omega'-\omega)+\mathrm{Im}G(\mathbf{k}-\mathbf{q},\omega')\mathrm{Re}G(\mathbf{k},\omega'+\omega)]\tanh\frac{\omega'}{2T}, \tag{4}$$

where the Green's function

$$G(\mathbf{k},\omega)=\frac{1}{\omega-E(\mathbf{k})-\Sigma(\mathbf{k},\omega)} \tag{5}$$

and $\Sigma(\mathbf{k},\omega)$ is the self-energy, $\Sigma=\Sigma'+i\Sigma''$. Following Ref. 7, we neglect the mass renormalization, i.e., $\Sigma'=0$; this allows a self-consistent determination of the imaginary part of the self-energy, giving $-\Sigma''(\omega)=\Gamma(\omega)=\mathrm{Max}(|\omega|,T)$. The expression for $\chi'(q,\omega)$ then reduces to

$$\chi'(\mathbf{q},\omega)=\frac{1}{(2\pi)^3}\int d\omega'\int d\mathbf{k}\left[\frac{-\Gamma(\omega')}{[\omega'-E(\mathbf{k})]^2+\Gamma^2(\omega')}\frac{\omega'-\omega-E(\mathbf{k}-\mathbf{q})}{[\omega'-\omega-E(\mathbf{k}-\mathbf{q})]^2+\Gamma^2(\omega'-\omega)}\right.$$
$$\left.+\frac{-\Gamma(\omega')}{[\omega'-E(\mathbf{k}-\mathbf{q})]^2+\Gamma^2(\omega')}\frac{\omega'+\omega-E(\mathbf{k})}{[\omega'+\omega-E(\mathbf{k})]^2+\Gamma^2(\omega'+\omega)}\right]\tanh\frac{\omega'}{2T}. \tag{6}$$

We calculate the above susceptibility for the band model of Eq. (2) using the Bi2212 parameter values at a fixed temperature of $T=100$ K. The zero-frequency susceptibility is plotted in Fig. 4 as a function of momentum $|\mathbf{q}|$ along the $q_x=q_y$ direction (solid curve). For comparison, we also plot the result for zero damping calculated earlier (dashed curve). One can see the peak structure at the nesting vector persists, though the magnitude of the susceptibility is smaller than the zero damping result at all q values.

The SDW constraint on the susceptibility requires $U\leq 1.1$ eV in the case of Bi2212, provided one considers the susceptibility renormalized by the self-energy. Since the peak heights decrease as a function of frequency, this bound is set by the static susceptibility whose maximum value occurs at the nesting vector $\mathbf{Q}^*$. We note that the peak structure at low frequencies is similar to the neutron spectra for the $La_{2-x}Sr_xCuO_4$ superconductor.[21] Another consequence of nesting is the scaling[7] of the spin susceptibility $\chi''(\mathbf{Q}^*,\omega)$ as a function of ω/T which has been confirmed by neutron scattering on several cuprates.[22]

The intermediate strength of the Coulomb coupling U that we invoke is comparable to the energy bandwidth $8t=1.5$ eV which was estimated from photoemission data.[10,11] Larger values of U are difficult to reconcile with these experiments and other photoemission data on the YBCO superconductors as well. Independent experimental evidence for intermediate U values includes the magnitude of the resistivity as discussed in Ref. 7, and the shapes of the optical reflectivity of various cuprates which are analyzed in Ref. 8. Theoretical groups that have also used intermediate U values include Refs. 11, 14, 15, and various references cited therein.

Nesting generally enhances the susceptibility and therefore the tendency to form spin-density waves.[23] Chromium[23,24] and various rare-earth metals exhibit nesting-induced peak structure in the susceptibility which leads to SDW states and other spin-ordering phenomena. Hence it is vital to find novel features of the Fermi-surface topology to distinguish the mechanism responsible for superconductivity in cuprates from other processes that create competing spin-correlation instabilities.

In calculating the pairing coupling between electrons it is useful to devise an analytic form for the susceptibility. We represent it by a Gaussian form

$$\chi'(\mathbf{q},0)=A+C\exp\left[-\frac{(|q_x|-Q_x)^2+(|q_y|-Q_y)^2}{2\alpha^2}\right], \tag{7}$$

where $\mathbf{q}=\mathbf{k}-\mathbf{k}'$, $\mathbf{Q}=(\pi,\pi)$, the constants A and C determine the normalization and α the width for the Gaussian. This model yields a reasonable fit to the computed Bi2212

susceptibility, as shown by the dot-dashed line in Fig. 4. Though the detailed calculations for the Bi2212 model indicate four nesting peaks in the two-dimensional structure of the susceptibility, we find that using a more sophisticated model which reproduces this four-peak structure makes only small corrections to the superconducting coupling constant determined by the simple Gaussian in Eq. (7). These results will be described in the next section.

In order to determine an appropriate cutoff for the spin-fluctuation exchange interactions, we calculate the susceptibility as a function of frequency ω. The result for the Bi2212 model parameters is shown by the solid curve in Fig. 5. The damping $\Gamma=\mathrm{Max}(|\omega|,T)$ suppresses the susceptibility at large ω, which suggests a cutoff in the range of $\omega_c=0.3$ eV. Also shown in Fig. 5 is the susceptibility (dashed curve) for a perfectly nested square Fermi surface that occurs at half-filling ($\mu=0$) if we set $B=0$ in our tight-binding model. In the square orbit case there is a logarithmic increase in χ' as $\omega\to 0$, since the Fermi energy coincides with the logarithmic Van Hove singularity in the density of states. This increase in χ' will drive the perfectly nested system into the SDW state for arbitrarily small values of the Coulomb interaction.

The density of states for the energy band model of Eq. (2) follows from the standard definition,

$$N(\omega)=\int \frac{d^2k}{(2\pi)^2}\delta[\omega-E(\mathbf{k})]\ . \tag{8}$$

A numerical evaluation of the phase-space integral in Eq. (8) leads to the density of states for the nested band shown in Fig. 6. It is interesting to note that the Fermi energy is located 0.04 eV $\simeq$500 K below the logarithmic Van Hove singularity for the Bi2212 model parameters.

III. SUPERCONDUCTIVITY

The presence of nesting in a two-dimensional band is detrimental to a BCS mechanism for superconductivity because the electron-phonon coupling favors a charge-density-wave instability instead of s-wave singlet pairing.[25] The enhanced spin fluctuations will also be detrimental to the binding of electron pairs in s states.[4]

The primary basis for the d-wave pairing we consider is the Berk-Schrieffer[4] process of exchange of spin fluctuations shown in Fig. 7. These consist of a direct Coulomb term and the spin-fluctuation graphs, where the electron-hole bubble represents the susceptibility.

Decomposition of the two-particle scattering into

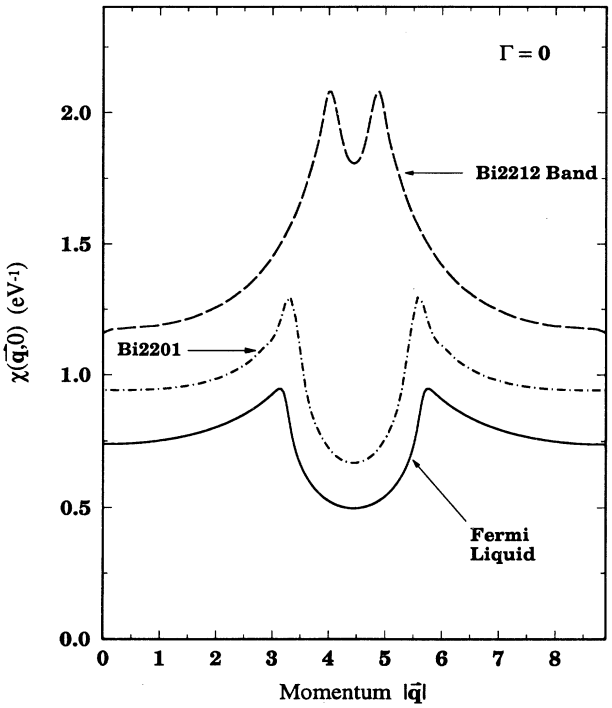

FIG. 3. The real part of the static susceptibility calculated from Eq. (3) for zero damping and at temperature $T=100$ K is shown as a function of momentum $|\mathbf{q}|$ along the direction $q_x=q_y$. The dashed curve is calculated using the Bi2212 band parameters $B=0.165$ and $\mu=-0.56$, and the solid curve represents the results for the FL parameters $B=0.165$, $\mu=-1.6$ that correspond to the rounded Fermi surface shown in the previous figure. The dot-dashed curve is the result for the Bi2201 band parameters $B=0.33$ and $\mu=-1.36$. The bandwidth is held fixed at $8t=1.5$ eV.

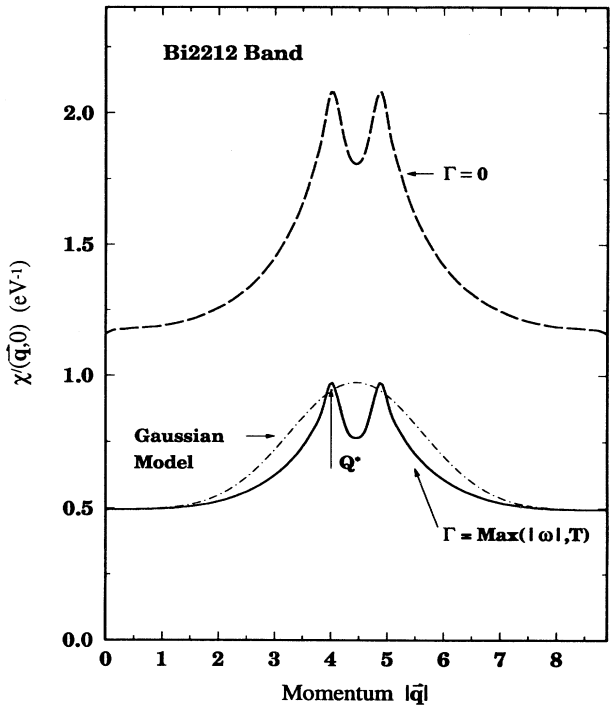

FIG. 4. The solid curve represents the calculated static susceptibility for the Bi2212 band parameters $B=0.165$ and $\mu=-0.56$, shown as a function of momentum $|\mathbf{q}|$ along the direction $q_x=q_y$ by including the damping $\Gamma_{\mathrm{NFL}}=\mathrm{Max}(|\omega|,T)$ where $T=100$ K [see Eq. (6)]. As a comparison, the result for zero damping is shown here by the dashed curve. The calculated maximum $\chi'(\mathbf{Q}^*)\simeq 0.97$ eV^{-1} constrains the interaction strength $U<1$ eV which compares with the bandwidth $8t=1.5$ eV that we estimated from the photoemission data of Ref. 10. The dot-dashed curve represents the Gaussian model of Eq. (7) with $\alpha=1.2$, $A=0.49$, and $C=0.476$.

angular-momentum channels yields an effective pairing coupling:[11]

$$\lambda_l = -\frac{\sum_{\mathbf{k}\mathbf{k}'} g_l(\mathbf{k})V(\mathbf{k},\mathbf{k}')g_l(\mathbf{k}')\delta[E(\mathbf{k})]\delta[E(\mathbf{k}')]}{\sum_{\mathbf{k}} g_l^2(\mathbf{k})\delta[E(\mathbf{k})]} . \quad (9)$$

The conventional symmetry classification of the basis set g_l (Refs. 11–15) is $g_s=1$ for s-wave states, $g_p=\sin k_x$ for p-wave, and $g_{x^2-y^2}=\cos k_x-\cos k_y$ and $g_{xy}=\sin k_x \sin k_y$ for d-wave states.

The primary pairing interaction $V(\mathbf{k},\mathbf{k}')$ (see Fig. 7) is given by the term with two spin-fluctuation bubbles, $U^3\chi'^2(\mathbf{k}-\mathbf{k}')$, and the exchange term proportional to $U^2\chi'(\mathbf{k}+\mathbf{k}')$. The direct Coulomb repulsion term vanishes in the d-wave channel because the Hubbard model presumes a point interaction in real space for the Coulomb repulsion. A standard Fermi-liquid example of a free-electron dispersion in two dimensions that gives rise to a constant susceptibility $\chi'(\mathbf{q},0)$, up to $2k_F$, will not be superconducting in the d-wave channel. The reason for the lack of attraction (i.e., $\lambda=0$) between a pair of electrons in this cylindrical Fermi surface case follows directly from the phase-space integration in Eq. (9).

Nesting of the Fermi surface creates an opportunity for d-wave pairing since the symmetry favors overlap of the positive and negative regions of the gap function. We

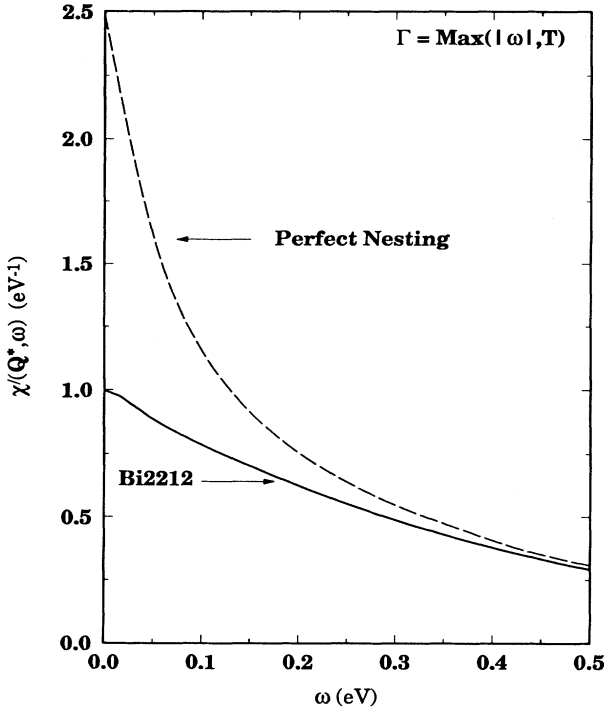

FIG. 5. The solid curve shows the real part of the susceptibility at the nesting vector $\mathbf{Q}^*=0.91(\pi,\pi)$ [Eq. (6)] for the Bi2212 model parameters plotted as a function of frequency, using the damping $\Gamma=\mathrm{Max}(|\omega|,T)$ with $T=100$ K. The dashed curve represents the result for a perfectly nested square Fermi surface with $B=\mu=0$ and $\mathbf{Q}^*=(\pi,\pi)$. In the latter case, the logarithmic increase in χ' as $T\to 0$ drives the system into the SDW regime even at small values of the Coulomb interaction strength U.

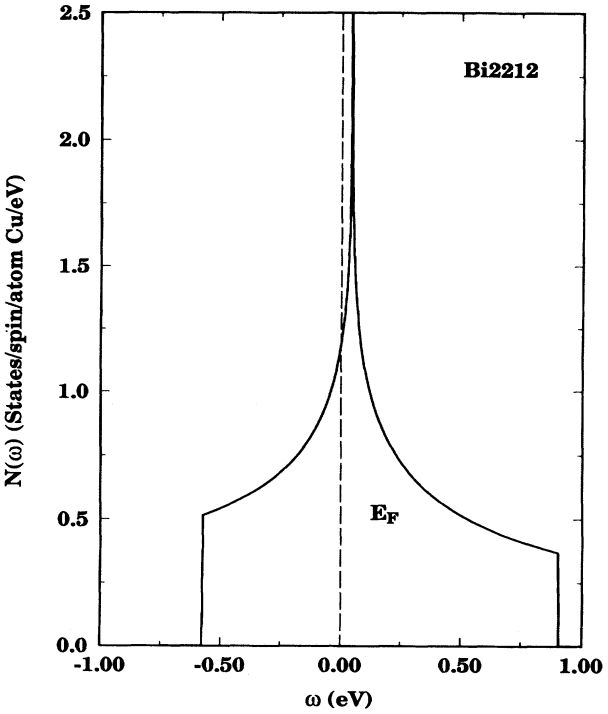

FIG. 6. The density of states for the Bi2212 model parameters $B=0.165$, $\mu=-0.56$, and bandwidth $8t=1.5$ eV. The location of the Fermi energy is indicated on the figure. Note that the logarithmic Van Hove singularity in the density of states is situated approximately 0.04 eV $\simeq$500 K above the Fermi energy.

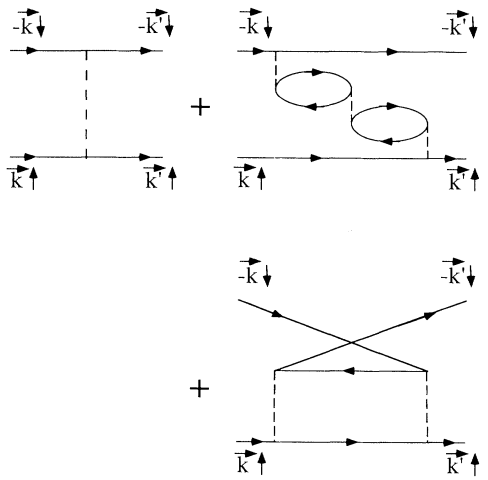

FIG. 7. Diagrams for the electron-electron scattering in the singlet channel show the direct Coulomb repulsion by a dotted line and the spin-fluctuation exchange processes with a bubble representing the susceptibility. In the d-wave channel for a nested Fermi surface, the leading-order attractive contributions from the graphs involving the susceptibility are of the same order, whereas the direct bare Coulomb repulsion gives no contribution in the Hubbard model, because U is assumed to be momentum independent.

proceed to compute the superconducting transition temperature for the realistic band model whose chosen orbit topology naturally links lobes of opposite sign of the $d_{x^2-y^2}$ states by virtue of the nesting vector direction along the $q_x=q_y$ direction. We use the Gaussian analytic form for the susceptibility given in Eq. (7), and evaluate the coupling constant $\lambda_{x^2-y^2}$ by numerical integration over momenta. As seen in Fig. 5, our computed susceptibility indicates an energy cutoff $\omega_c \simeq 0.3$ eV for the spin-fluctuation exchange process. An upper limit on a cutoff is set by the energy scale of the bandwidth $8t=1.5$ eV. Our conservative choice of 0.3 eV is the frequency where the calculated susceptibility decreases to half of its static value, as shown for Bi2212 in Fig. 5. Numerical calculations for the FL parameter set yield a similarly smooth susceptibility decline, which indicates that the cutoff is relatively insensitive to the shift of the chemical potential which distinguishes the FL case from Bi2212. A similar value of ω_c is obtained for the Bi2201 parameters, which suggests that the cutoff varies weakly with this change in B. However, the overall magnitudes of the susceptibility as a function of frequency follow the trends for the static susceptibility seen in Fig. 3. In our leading-order analysis the cutoff does not depend on U. The leading-order evaluation of the superconducting temperature gives

$$T_c=\omega_c \exp\left[-\frac{1}{\lambda_{x^2-y^2}}\right]. \tag{10}$$

The clear benefit for achieving high-temperature superconductivity by means of a spin-fluctuation mechanism is the prefactor $\omega_c \simeq 0.3$ eV $\simeq 2500$ K. However, the dilemma is to find a way to achieve a substantial coupling $\lambda > 0.1$, since the exponential dependence seen in Eq. (10) will otherwise suppress T_c to negligibly small values for weaker coupling.

A. Fermi liquid

We first test the case of an ordinary Fermi-liquid topology without nesting for comparison with previous calculations using tight-binding models.[11–15] Spin fluctuations generate a net repulsion of electrons and therefore suppress superconductivity in the standard parabolic band model as shown by Berk and Schrieffer.[4] Therefore we consider a tight-binding model better suited to cuprates and use the Fermi liquid (FL) label to distinguish cases with rounded orbits that are expected to exhibit a characteristic T^2 variation of the electron-electron cross section. Using the energy band parameters that produce the dashed curve (FL) Fermi surface shown in Fig. 2 we compute the susceptibility for zero damping (as shown in Fig. 3) and then compute T_c. Choosing a Coulomb interaction $U=0.95$ eV that is close to the highest value permitted by the SDW constraint, and approximating $\chi'(q)$ by the Gaussian model of Eq. (7), we find $\lambda_{\rm FL}=0.037$ and $T_c=0$. An analytic representation of the susceptibility that models the dip between the nesting peaks more accurately by a parabola leads to a $\lambda_{\rm FL}=0.054$ which also corresponds to a vanishing T_c. This example is qualitatively similar to other cases studied by several groups,[11–15] and our conclusions regarding an inadequate superconducting pairing in leading order are consistent with the earlier work. Although random-phase-approximation (RPA) contributions selectively enhance this coupling near the SDW instability,[11,13–15] a reliable estimate of such higher-order contributions requires a full scale examination of self-energy and vertex corrections which is beyond the scope of the present work.

B. Nesting

Nested segments of the Fermi surface provide a twofold benefit for creating a superconducting state of d-wave symmetry that persists up to the 155-K range of T_c values that have been discovered so far in the cuprates. The first and obvious advantage of nesting is the enhanced peak structure in the susceptibility evident in the calculated curves in Figs. 3 and 4. Although perfect nesting would give rise to the largest susceptibility, it is not suitable for superconductivity since such a square orbit would trigger a SDW instability instead. Thus, the present model for Bi2212 offers a realistic hope for achieving superconductivity since the rounded corners of the nested surface shown in Fig. 2 lower the density of states at the Fermi energy and also suppress the SDW instability by reducing the value of the susceptibility near the nesting vector $\mathbf{Q}^*$.

The novel advantage of nesting that we find here is the beneficial influence of the nesting topology in the phase-space integrals of Eq. (9) which determine the pairing attraction. We thus obtain by direct computation for the Bi2212 parameters that the leading-order spin-exchange processes along with the susceptibility shown in Fig. 4 give $\lambda_{x^2-y^2}=0.27$ and a superconducting transition temperature of $T_c=89$ K if we choose $U\chi'_{\rm max}=0.93$ which requires a Coulomb repulsion $U=0.95$ eV for our calculated $\chi'_{\rm max}=0.97$ eV^{-1}. Since the bandwidth for our model is $8t=1.5$ eV, the requisite Coulomb interaction is of intermediate strength.

Quantitative accuracy of course requires rigorous treatment of higher-order corrections, and we hope that our novel and surprising results for the lowest-order coupling will stimulate further theoretical research along these lines.

A fundamental mystery is the surprising disparity in T_c values for Bi2212 ($T_c=85$ K) and Bi2201 ($T_c=6$ K). This needs to be reconciled with the fact that both of these compounds exhibit the anomalous linear temperature dependence of the resistivity and strong deviations from Drude behavior of the optical properties. We were motivated to understand this dilemma by the discovery of King *et al.*[18] that both of these compounds have nested Fermi surfaces, but with nesting vectors that differ by roughly 10%. Thus we were led to examine the sensitivity of the d-wave transition temperature T_c to the magnitude of the nesting vector by direct numerical analysis, which is shown in Fig. 8. Our computations reveal a dramatically steep rise in T_c (solid curve) as the nesting vector reaches $\mathbf{Q}^* \simeq 0.91\mathbf{Q}$ which corresponds to the Bi2212 Fermi surface shown in Fig. 2 if $\mathbf{Q}=(\pi,\pi)$. If the nesting vector is reduced to $\mathbf{Q}^* \simeq 0.8\mathbf{Q}$ and if U is held constant, the calculated T_c falls below 10 K, and rapidly

approaches zero for even smaller $\mathbf{Q}^*$. This behavior of T_c resulting from the nesting mechanism is compatible with the photoemission evidence[18] for a reduced $\mathbf{Q}^*$ value in Bi2201. The SDW region that constrains our model band structure is also shown in Fig. 8 by the shaded area which marks the nesting vector range that would trigger a SDW instability for the value of $U=0.95$ eV chosen here.

Finally we examine the sensitivity of the Bi2212 model to changes in the chemical potential μ while keeping the other band-structure parameters constant. It is remarkable that the present model that includes next-nearest-neighbor tight-binding interactions retains nesting features over a significant range of chemical potential shifts in the particular case of the B and t parameters used here, as seen in Fig. 9. This persistence of nesting is in sharp contrast with the simpler tight-binding model[22] with only nearest-neighbor orbital overlaps whose nesting features are spoiled by small changes in μ. A direct numerical check confirms that the nesting approximation $E(\mathbf{k}+\mathbf{Q})+E(\mathbf{k})\leq k_B T$ is satisfied by major segments of the Fermi surface shown in Fig. 9. These are then compatible with the NFL derivation of the linear T and ω damping which explains a key feature of the cuprates. Other studies have used different model Hamiltonians, alternate band models, and a variety of parameter sets. It

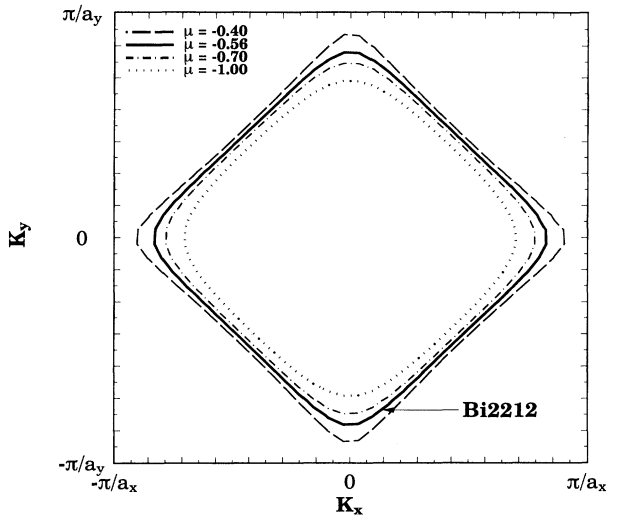

FIG. 9. Fermi surfaces of the Bi2212 energy band model [Eq. (2)] for different values of the chemical potential μ. The parameter $B=0.165$ is held fixed. The solid curve represents the Bi2212 Fermi surface with $\mu=-0.56$, the dashed curve is for $\mu=-0.4$, the dot-dashed curve for $\mu=-0.7$, and the dotted curve for $\mu=-1.0$. As μ becomes more negative, the Fermi surface becomes smaller and more rounded.

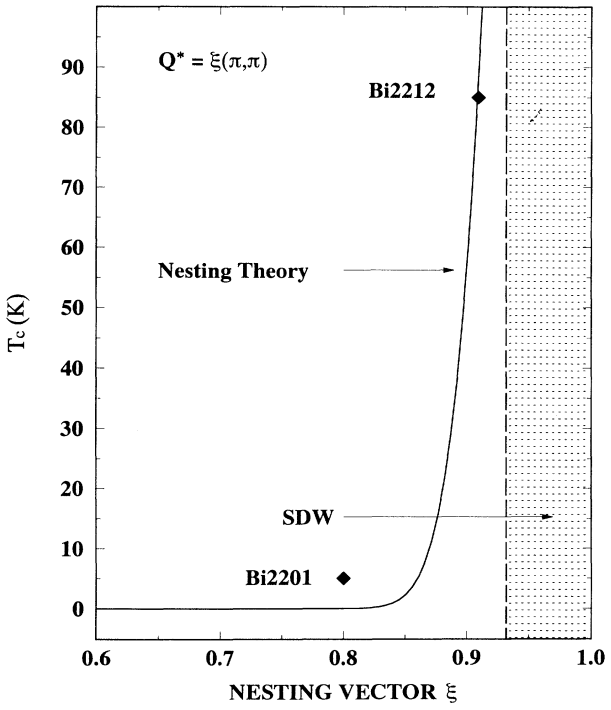

FIG. 8. T_c values as a function of the nesting vector $\mathbf{Q}^*$ calculated using the tight-binding model of Eq. (2) are shown by the solid curve. The Bi2212 parameters are $B=0.165$ and $\mu=-0.56$, $U=0.95$ eV, and a bandwidth $8t=1.5$ eV. The points are the experimental values. A surface with a nesting vector $\mathbf{Q}^*\simeq 0.8(\pi,\pi)$ appropriate to the Bi2201 photoemission data (Ref. 18) was simulated using $B=0.33$ and $\mu=-1.36$ which lowers T_c. Intermediate $\mathbf{Q}^*$ cases were found by linear interpolation of the band structure.

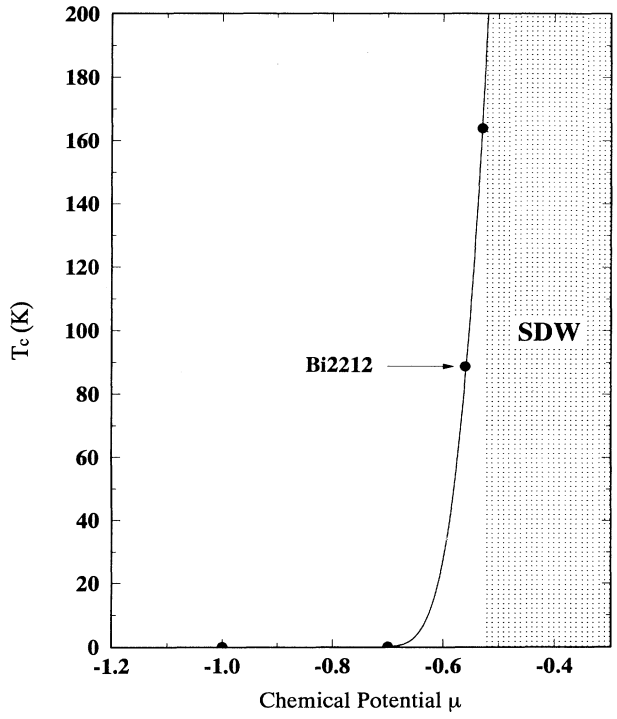

FIG. 10. Calculated T_c values are plotted as a function of the chemical potential μ using the tight-binding model of Eq. (2). The parameters $U=0.95$ eV, bandwidth $8t=1.5$ eV, and $B=0.165$ are held fixed. The value $\mu=-0.56$ corresponds to the Bi2212 case, while some of the other points are at the values of μ corresponding to the Fermi surfaces shown in Fig. 9. The shaded region designates the spin-density-wave (SDW) regime; the case $\mu=-0.4$ is in this regime. The Gaussian fit parameters are shown in Table I.

TABLE I. Gaussian fit parameters used in the calculation of T_c as a function of μ (see Fig. 10). The Fermi-liquid (FL) susceptibility is calculated for zero damping.

μ	A (eV^{-1})	C (eV^{-1})	α	T_c (K)
−1.60 (FL)	0.737	0.210	1.60	0
−1.00	0.350	0.210	1.25	0
−0.70	0.430	0.240	1.25	0.07
−0.56 (Bi2212)	0.494	0.476	1.20	89
−0.53	0.508	0.522	1.19	164
−0.40	0.630	0.780	0.80	SDW

would be interesting to see how other models may generate nesting and influence the superconducting pairing caused by spin fluctuations.

Changes in oxygen content or chemical composition that serve to shift the Fermi energy will influence the d-wave superconductivity even though the nesting may persist. This phenomenon is illustrated in Fig. 10 which shows the computed superconducting T_c values as a function of μ for the present band model. The nesting topology is the key determinant of T_c in this case. The relevant parameters (α, A, C) employed in the Gaussian fit are listed in Table I.

Elimination of nesting features by doping will destroy the present mechanism for d-wave superconductivity and cause the electrical transport properties to revert to conventional Fermi-liquid behavior. This type of correlation is seen experimentally[26] in the $Tl_2Ba_2CuO_{6+\delta}$ cuprate which exhibits $T_c = 85$ K and a linear T resistivity for $\delta = 0$ but becomes nonsuperconducting at $\delta = 0.1$ and develops a T^2 resistivity that persists up to room temperatures.

We do not find superconductivity of xy symmetry for our Fermi-surface geometry. The favored $x^2 - y^2$ state for the present nesting model is consistent with photoemission measurements of the energy gap anisotropy in Bi2212.[10] If the Fermi surface is rotated in other cuprates, as suggested by photoemission spectra of $YBa_2Cu_3O_{7-\delta}$ by Liu *et al.*,[27] then states of other symmetry should be examined in more detail. We find a vanishing T_c for p-wave symmetry pairing using $g_x = \sin k_x$ in both the Fermi-liquid model and the nested Fermi-surface case.

Impurity scattering should be detrimental to anisotropic pairing as well as for the SDW formation. By analogy with the Abrikosov-Gorkov theory,[28] d-wave suppression by disorder constrains T_c in the cuprates.[29] Similarly, nonmagnetic impurities also impede the competing SDW transition.[30] The case of chromium reveals a further sensitivity of the SDW to impurity induced shifts of the band structure[31] which may also occur in the cuprates. Impurities at sites in the copper-oxide planes should presumably be more destructive for d-wave superconductivity than those at interplanar sites. An extension of the present model to include impurity effects is surely warranted.

The origin of nesting features in cuprates is evident in band-structure calculations[32] because of the nearly half-filled d bands in two dimensions. The relative persistence of parallel segments in a given band subjected to doping may be also stabilized by a second band that acts as a charge reservoir. Photoemission data support the existence of multiple bands in YBCO (Ref. 27) and in BSSCO.[9]

IV. CONCLUSIONS

We have found that nested regions of the Fermi surface produced by a realistic tight-binding energy band model can yield superconductivity at very high temperatures. The necessary ingredients for the d-wave symmetry pairing mechanism are a Coulomb repulsion of intermediate strength, nesting vectors whose magnitudes are restricted to a narrow range, and a nearly two-dimensional nested Fermi-surface topology.

Since our band model is tailored to resemble the Fermi surface of Bi2212 unveiled by recent photoemission data,[9,10] there is an empirical constraint on the on-site Coulomb repulsion U that is imposed by the spin-density-wave instability. We find that values of U that are close to but less than the bandwidth are suitable for producing a d-wave superconducting state while avoiding a transition to the SDW phase. Thus our present analysis of the spin susceptibility for a realistic Fermi surface in the Bi2212 cuprates establishes an upper limit on U that may provide a useful guide for other theoretical approaches to metallic cuprates.

A novel feature of the nesting mechanism is the ability to generate high-T_c values above 100 K in the leading-order treatment of spin-fluctuation processes. Our analysis yields negligible values of T_c in the same lowest-order graphs if the nesting topology is removed by changing the chemical potential to produce rounded Fermi-liquid-like structures, and the latter cases are in qualitative agreement with previous calculations.[11–15] However, higher-order self-energy and vertex corrections need to be examined in any event.

Our model distinguishes the high-T_c (=85 K) Bi2212 cuprate from the low-T_c (=6 K) Bi2201 compound on the basis of a 10% change in the magnitude of the nesting vector which has been observed by King *et al.*[18] This remarkable sensitivity of the calculated d-wave T_c is a direct result of the Fermi-surface topology, while the presence of nesting in both these bismuth-based cuprates is compatible with their electrical[7] and optical[8] transport anomalies. More generally, the nesting mechanism provides a direct link to the linear T variation of the resistivity which has been a puzzling feature of all of the very high-T_c superconductors found to date.

Theoretical extensions of the present work may be relevant to higher-order spin-fluctuation graphs, including the "spin-bag" variety.[33] Nesting of a two-dimensional electronic structure produces[7,8] a linear frequency variation of the quasiparticle damping that bears similarities to the Luttinger theory[34] for a one-dimensional electron gas, which is known to exhibit unusual charge and spin dynamics.[35,36]

Nevertheless, nesting in two dimensions is dis-

tinguished by a crossover temperature T^* below which the electronic response reverts to standard Fermi-liquid behavior because a finite curvature of an electron trajectory is expected in a realistic situation. Accordingly, the concept of a well-defined Fermi surface is valid in the NFL approach, despite the unusual damping features that arise above T^* and at frequencies above a corresponding crossover ω^* determined by the nesting geometry.

ACKNOWLEDGMENTS

We have benefited from discussions with J. P. Collman, D. S. Dessau, D. Huse, R. B. Laughlin, W. A. Little, and Z. X. Shen. We (J.R. and C.R.) appreciate the hospitality of the Physics Department at Stanford University during a visit sponsored by the University of Virginia. Research supported by DOE Grant No. DE-FG05-84ER45113 and by HNRF Grants Nos. OTKA 2950 and T4473.

---

*Present address: Abteilung für Theoretische Festkörperphysik, Universität Hamburg, Hamburg, Germany.

[1]J. Bardeen, L. N. Cooper, and J. R. Schrieffer, Phys. Rev. **108**, 243 (1957).
[2]P. W. Anderson and P. Morel, Phys. Rev. **123**, 1911 (1961).
[3]S. Doniach and S. Engelsberg, Phys. Rev. Lett. **17**, 750 (1966).
[4]N. F. Berk and J. R. Schrieffer, Phys. Rev. Lett. **17**, 433 (1966).
[5]A. J. Leggett, Rev. Mod. Phys. **47**, 331 (1975).
[6]P. A. Lee and N. Read, Phys. Rev. Lett. **58**, 2692 (1987).
[7]A. Virosztek and J. Ruvalds, Phys. Rev. B **42**, 4064 (1990).
[8]J. Ruvalds and A. Virosztek, Phys. Rev. B **43**, 5498 (1991).
[9]D. S. Dessau *et al.*, Phys. Rev. Lett. **71**, 2781 (1993).
[10]Z. X. Shen *et al.*, Phys. Rev. Lett. **70**, 1553 (1993).
[11]D. J. Scalapino, E. Loh, Jr., and J. E. Hirsch, Phys. Rev. B **34**, 8190 (1986); **35**, 6694 (1987); H. Q. Lin, J. E. Hirsch, and D. J. Scalapino, *ibid.* **37**, 7359 (1988).
[12]J. E. Hirsch, Phys. Rev. Lett. **54**, 1317 (1985).
[13]M. Kato and K. Machida, Phys. Rev. B **37**, 1510 (1988).
[14]H. Shimahara and S. Takada, J. Phys. Soc. Jpn. **57**, 1044 (1988).
[15]R. Putz, B. Ehlers, L. Lilly, A. Muramatsu, and W. Hanke, Phys. Rev. B **41**, 853 (1990).
[16]V. J. Emery, Synth. Met. **13**, 21 (1986).
[17]H. R. Ott, H. Rudiger, T. M. Rice, K. Ueda, and J. L. Smith, Phys. Rev. Lett. **52**, 1915 (1984); K. Miyake, S. Schmitt-Rink, and C. M. Varma, Phys. Rev. B **34**, 6554 (1986).
[18]D. M. King *et al.*, Phys. Rev. Lett. **73**, 3298 (1994).
[19]Q. Si, Y. Zha, K. Levin, and J. P. Lu, Phys. Rev. B **47**, 9055 (1993); P. B. Littlewood, J. Zaanen, G. Aeppli, and H. Monien, *ibid.* **48**, 487 (1993).
[20]A. A. Abrikosov, L. P. Gorkov, and I. E. Dzyaloshinski, *Methods of Quantum Field Theory in Statistical Physics* (Prentice-Hall, New Jersey, 1963), p. 179.
[21]T. E. Mason *et al.*, Phys. Rev. Lett. **71**, 919 (1993), and references cited therein.
[22]J. Ruvalds *et al.*, Science **256**, 1664 (1992), and references cited therein.
[23]A. W. Overhauser, Phys. Rev. **128**, 1437 (1962).
[24]E. Fawcett, Rev. Mod. Phys. **60**, 209 (1988); W. M. Lomer, Proc. Phys. Soc. London **80**, 489 (1962).
[25]C. A. Balseiro and L. M. Falicov, Phys. Rev. B **20**, 4457 (1979).
[26]Y. Kubo, Phys. Rev. B **43**, 7875 (1991).
[27]Rong Liu *et al.*, Phys. Rev. B **46**, 11 056 (1992).
[28]A. A. Abrikosov and L. P. Gorkov, Zh. Eksp. Teor. Fiz. **39**, 1781 (1960) [Sov. Phys. JETP **12**, 1243 (1961)].
[29]A. Millis *et al.*, Phys. Rev. B **37**, 4975 (1988).
[30]J. Zittartz, Phys. Rev. **164**, 575 (1967).
[31]R. S. Fishman and S. H. Liu, Phys. Rev. B **45**, 12 306 (1992).
[32]W. E. Pickett, Rev. Mod. Phys. **61**, 433 (1989), and references cited therein.
[33]A. Kampf and J. R. Schrieffer, Phys. Rev. B **41**, 6399 (1990).
[34]J. M. Luttinger, Phys. Rev. **121**, 942 (1961).
[35]J. Solyom, Adv. Phys. **28**, 201 (1979).
[36]P. W. Anderson, Phys. Rev. Lett. **67**, 2092 (1991); Science **235**, 1196 (1987).